

The FLAMINGO project: Baryon effects on the matter power spectrum

Matthieu Schaller^{1,2}★, Joop Schaye², Roi Kugel², Jeger C. Broxterman^{1,2} & Marcel P. van Daalen²

¹Lorentz Institute for Theoretical Physics, Leiden University, PO Box 9506, NL-2300 RA Leiden, The Netherlands

²Leiden Observatory, Leiden University, PO Box 9513, NL-2300 RA Leiden, The Netherlands

Accepted XXX. Received YYY; in original form ZZZ

ABSTRACT

The effect of baryon physics associated with galaxy formation onto the large-scale matter distribution of the Universe is a key uncertainty in the theoretical modelling required for the interpretation of Stage IV cosmology surveys. We use the FLAMINGO suite of simulations to study the baryon response due to galaxy formation of the total matter power spectrum. We find that it is only well converged for simulation volumes in excess of 200^3 Mpc³. We report results for simulations of varying feedback intensity, which either match the X-ray inferred gas fractions in clusters and the $z = 0$ stellar mass function, or shifted versions of the data, as well as for different implementations of AGN feedback. We package our results in the form of a Gaussian process emulator which can rapidly reproduce all the simulations’ predictions to better than 1% up to the comoving wavenumber $k = 10 h \cdot \text{Mpc}^{-1}$ and up to $z = 2$ for all the feedback models present in the FLAMINGO suite. We find that the response becomes stronger, the range of scales affected increases, and the position of the minimum of the response moves to smaller scales as the redshift decreases. We find that lower gas fractions in groups and clusters lead to a stronger response and that the use of collimated jets instead of thermally driven winds for AGN feedback enhances the effect. Lowering the stellar masses at fixed cluster gas fractions also increases the magnitude of the response. We find only a small (1% at $k < 10 h \cdot \text{Mpc}^{-1}$) dependence of our results on the background cosmology, but a wider range of cosmology variations will be needed to confirm this result. The response we obtain for our strongest feedback models is compatible with some of the recent analyses combining weak lensing with external data. Such a response is, however, in strong tension with the X-ray inferred gas fractions in clusters used to calibrate the FLAMINGO model.

Key words: large-scale structure of Universe – cosmology: theory – methods: numerical

1 INTRODUCTION

Over nearly three decades, our standard model of cosmology, the Λ CDM model, has received substantial scrutiny from the community and successfully passed a multitude of stress tests (see e.g. [Dodelson & Schmidt 2020](#); [Lahav & Liddle 2022](#)). This vast program, designed to find faults in the model, understand its limitations, and identify possible extensions is continuing in this decade with exceedingly demanding precision tests, generally grouped under the “Stage IV cosmology probe” label. Many of these tests are focusing on the growth of the large scale structure (LSS) and are providing independent constraints from the geometric probes, such as the baryon acoustic oscillations (BAO) or Type Ia supernovae, or the analysis of fluctuations of the cosmic microwave background (CMB). Most of these programs were designed to shed some light on the nature of both dark matter and dark energy as well as to explore some of the tensions currently emerging between orthogonal probes (see e.g. [Abdalla et al. 2022](#)).

The many different LSS tests (e.g. cosmic shear, galaxy clustering, redshift-space distortions, CMB lensing, Sunyaev–Zel’dovich power spectra, and combinations thereof) probe the matter content of the Universe and its distribution across many different length-scales and at multiple epochs throughout cosmic time. As the scales

probed become smaller with each generation of instruments, the challenge of making accurate theoretical predictions grows. Many of the probes mentioned above are now exploiting information well into the non-linear regime, where perturbation theory is not sufficient anymore. The main approach used over the last twenty years has been to resort to the “halo model” analytic formalism (e.g. [Seljak 2000](#); [Smith et al. 2003](#); [Asgari et al. 2023](#)) itself (usually) calibrated on the results of N -body simulations (e.g. [Takahashi et al. 2012](#); [Mead et al. 2016](#)). More recently, the ability to run a sufficiently large number of cosmological simulations has allowed an alternative approach based on the direct interpolation between simulations (typically via emulators) to predict many quantities required for data analysis (e.g. [Heitmann et al. 2016](#); [Lawrence et al. 2017](#); [DeRose et al. 2019](#); [Euclid Collaboration et al. 2019](#); [Bocquet et al. 2020](#); [Angulo et al. 2021](#); [Storey-Fisher et al. 2024](#)).

Both the halo model and emulators trained on pure N -body simulations would suffice if the scales probed were not affected by the behaviour of baryons. Whilst on large scales, $k \lesssim 0.1 h \cdot \text{Mpc}^{-1}$, the joint baryon and dark matter fluid behaves similarly to a pure dark matter model (with initial conditions accounting for BAO), studies based on simulations including hydrodynamics and galaxy formation effects have shown that the matter field on smaller scales deviates significantly from the pure N -body predictions (e.g. [van Daalen et al. 2011, 2020](#); [Schneider & Teyssier 2015](#); [Mummery et al. 2017](#); [Springel et al. 2018](#); [Salcido et al. 2023](#); [Pakmor et al. 2023](#); [Schaye](#)

* E-mail: mschaller@lorentz.leidenuniv.nl

et al. 2023) and that neglecting this effect will result in catastrophic systematic errors (e.g. Semboloni et al. 2011). The amplitude of the baryonic effect depends on uncertain feedback processes and is thus difficult to predict. However, the amplitude is understood to depend on observables such as the baryonic content of groups and clusters (e.g. Semboloni et al. 2011, 2013; van Daalen & Schaye 2015; Chisari et al. 2019; van Daalen et al. 2020; Mead et al. 2020; Salcido et al. 2023; van Loon & van Daalen 2024) and halo models reproducing these observables confirm the importance of baryon effects (Debackere et al. 2020). The modelling of these deviations, commonly referred to as “baryon effects”, is crucial for the interpretation of future surveys probing the matter distribution deep into the non-linear regime.

Thanks to its speed and flexibility, the community’s preferred approach thus far, has been to use relatively simple analytic prescriptions to correct the predictions of N -body simulations (e.g. Schneider & Teyssier 2015; Aricò et al. 2021) or halo models (e.g. Mead et al. 2021). These correction procedures themselves come with free parameters which could, in principle, be marginalised over when inferring cosmological information from survey data (e.g. Asgari et al. 2021; Aricò et al. 2023; Bigwood et al. 2024). Whilst being powerful, these extended halo models and other “baryonification” procedures also come with some drawbacks. The most important ones being the relatively simple nature of the models and the implicit assumption that the baryon physics is independent of the chosen background cosmology. These models also do not come with a clear ab-initio prediction for the strength of the correction required, though attempts have been made to link some of their parameters to observables to restrict the range of valid input parameters (e.g. Schneider & Teyssier 2015; Mead et al. 2020; Debackere et al. 2020; Schneider et al. 2022; Tröster et al. 2022; Aricò et al. 2023).

An alternative approach is to exploit hydrodynamical simulations. Their cost is much larger than the evaluation of corrective methods, but recent advances have allowed for large suites of simulations that vary the input parameters of their sub-grid models to be run (e.g. Le Brun et al. 2014; McCarthy et al. 2017; Villaescusa-Navarro et al. 2021; Salcido et al. 2023; Schaye et al. 2023). Among the advantages of this approach are the self-consistent nature of the modelling and the relative ease with which the simulated data can be connected to observables.

Whilst knowing and understanding the exact feedback mechanisms in galaxies would provide an ab-initio prediction for the properties of groups and clusters and thus of the baryon effect on the matter power spectrum, this is far beyond our current understanding of galaxy formation. Numerical simulations thus come with sub-grid recipes which are calibrated to match specific observables. The natural choice, based on the discussion above, is to target the gas or baryon fractions in groups and clusters of galaxies. The BAHAMAS (McCarthy et al. 2017), FABLES (Henden et al. 2018), and ANTILLES (Salcido et al. 2023) projects all took this approach to set the value of their free parameters. Thanks to the rather large simulation volumes probed, the effects of galaxy formation on the matter power spectrum from the COSMO-OWLS and BAHAMAS simulations are often used as references for the range of possible outcomes (e.g. Amon & Efstathiou 2022; Preston et al. 2023). They have also been used as input to some of the simpler corrective models described above (e.g. Mead et al. 2021; Aricò et al. 2023). Running large suites of simulations varying parameters around the best-fitting model is possible, but a more efficient approach to restrict the plausible parameter space is to build on the work of van Daalen et al. (2020). By analysing virtually all simulations from the literature at the time and building on the results from Semboloni et al. (2011, 2013), they for-

malised robustly the connection between group and cluster baryonic content and the effect of baryons on the matter power spectrum. Salcido et al. (2023) built on this idea to construct an emulator trained on the 400 simulations of their ANTILLES suite to predict the baryonic response of the matter power spectrum as a function of various combinations of cluster properties. Their emulation approach relating the unknown effect to some (almost) observable quantities allows to use their tool in cosmology inference (thanks to its speed) whilst providing meaningful data-driven priors.

In this study, we follow similar steps using the FLAMINGO suite of cosmological simulations (Schaye et al. 2023; Kugel et al. 2023). These simulations cover much larger simulated volumes than the ANTILLES suite and have been calibrated, using modern machine-learning-based techniques, to reproduce the observed *gas fractions* in groups and clusters. Whilst the connection to the power spectrum is less direct for the gas fraction, it is more easily observable than the total baryon fraction and the gas fraction is typically much larger than the stellar fraction for the relevant halo masses. The FLAMINGO simulations have been shown to reproduce a series of observables of the cluster population (Schaye et al. 2023; Braspenning et al. 2024; Kay et al. 2024) and thus offer a good baseline for the understanding of the effect of baryons on the matter power spectrum. Furthermore, the use of variations of the base model, where the observables have been shifted in a systematic fashion (Kugel et al. 2023), allows for a direct connection between the baryonic response and the observables the simulations were calibrated to. Additionally, the simulations themselves have already been used to investigate the role of baryons on the so-called S8 tension (McCarthy et al. 2023, 2024; Elbers et al. 2024). In this paper, we construct a simple and fast Gaussian process emulator predicting the baryon effects on the power spectrum as a function of redshift and simulation calibration targets. By publicly releasing our emulator, we provide a simple and efficient way of incorporating the results of the FLAMINGO suite of simulations in analysis pipelines of upcoming surveys.

This paper is organised as follows. In Sec. 2, we introduce the simulation model used and verify the convergence of the results with the simulation volume. In Sec. 3, we describe the procedure used to construct our baryon response emulator and validate it. In Sec. 4, we explore some results obtained using the emulator. Finally, we offer some conclusions in Sec. 5.

2 SIMULATIONS & POWER-SPECTRA MEASUREMENTS

In this section, we present the simulations used for this study (§2.1), describe how the matter power spectra are measured (§2.2) and analyse the convergence of the results (§2.3).

2.1 The FLAMINGO suite of simulations

The FLAMINGO simulations and the strategy used to calibrate their free parameters to match relevant observables are described in Schaye et al. (2023) and Kugel et al. (2023). We provide here a brief summary of the key components.

The simulations were performed using the SWIFT simulation code (Schaller et al. 2024)¹, a fully open-source coupled cosmology, gravity, hydrodynamics, neutrino & galaxy formation code. The gravity is solved using a 4th-order fast-multipole-method (FMM, see e.g.

¹ Publicly available, including the exact version used for the FLAMINGO simulations, at www.swiftsim.com.

Cheng et al. 1999) coupled to a Particle-Mesh method in Fourier space for the long-range interactions using the splitting method of (Bagla & Ray 2003). Cosmological neutrinos are evolved using the δf -method of Elbers et al. (2021). The equations of hydrodynamics are evolved using the SPHENIX (Borrow et al. 2022) flavour of Smoothed Particle Hydrodynamics (SPH).

The hydrodynamical simulations include subgrid prescriptions for radiative cooling following Ploekinger & Schaye (2020), an entropy floor at high densities and star formation using the method of Schaye & Dalla Vecchia (2008), stellar feedback using kinetic winds (Dalla Vecchia & Schaye 2008; Chaikin et al. 2022), and the chemical enrichment model of Wiersma et al. (2009). Supermassive black holes and thermally driven AGN feedback are modeled following Springel et al. (2005), Booth & Schaye (2009) and Bahé et al. (2022). The models with “jet” AGN feedback (see below) alternatively use the method of Huško et al. (2022) to produce feedback using collimated jets.

As is the case in all galaxy formation models, the simulations of the FLAMINGO suite have free parameters in their subgrid recipes. The approach chosen for this project to calibrate the feedback parameters was to construct a Gaussian process emulator, trained on a Latin hypercube of simulations, to predict the observables as a function of the subgrid parameters. This emulator was then used to calibrate the models against observational data, as presented in detail by Kugel et al. (2023). The simulations were chosen to reproduce the $z = 0$ galaxy stellar mass function as well as the gas fractions in groups and clusters inferred from X-ray and weak-lensing data. This choice is similar to the one made for the BAHAMAS simulations (McCarthy et al. 2017) but using a more systematic approach via the emulator.

Besides its added objectivity over calibration by hand, the use of an emulator to set the free parameters of the model offers an additional advantage: the possibility to rapidly generate simulated models where the data is shifted by particular amounts with respect to observations. In the case of the cluster gas fractions, we created different models where the observed gas fractions are shifted up and down compared to the results by $\pm N\sigma$, where σ is the scatter in the data (see Kugel et al. 2023, for the exact definitions). Once the emulator has been fitted to these shifted data points, we run a full simulation using the predicted subgrid parameter values. These simulations are labelled as “fgas $\pm N\sigma$ ” in Table 1. Similarly, we generated models fitting shifted versions of the stellar mass function, effectively lowering/increasing the mass of every galaxy by $\pm N\sigma$, where, σ is the systematic error on the measurements. These runs are labeled as “ $M_* \pm N\sigma$ ” in Table 1. Finally, we ran two simulations using the jet model of AGN for two different shifts of the gas fractions. These runs are labelled as “Jet fgas $\pm N\sigma$ ” in Table 1.

Outside of the tests in §4.3, the simulations used in this study adopt as values of the cosmological parameters the maximum likelihood values from the DES year 3 data release (Abbott et al. 2022) combined with external probes (their ‘3x2pt + All Ext.’ model: $\Omega_m = 0.306$, $\Omega_b = 0.0486$, $\sigma_8 = 0.807$, $h = 0.681$, $n_s = 0.967$, $\sum m_\nu c^2 = 0.06\text{eV}$). The initial conditions (ICs) were generated using the MONOFONIC code (Hahn et al. 2021; Elbers et al. 2022) using a 3-fluid formalism with a separate transfer function for each of the dark matter, gas, and neutrinos. The ICs used partially fixed modes (Angulo & Pontzen 2016), setting the amplitudes of modes with $(kL)^2 < 1025$ to the mean variance, where L is the side-length of the simulated box and k the modes’ wave-number. The multi-fluid approach (Rampf et al. 2021) used by MONOFONIC allows to obtain a perfect match of the gravity-only and full-hydrodynamics power spectrum on the largest scales.

Table 1. The nine different simulations of the FLAMINGO suite used in this study. All models assume the same cosmology and were run in 1 Gpc^3 volumes using the same initial conditions. The first column gives the simulation names used by Schaye et al. (2023). The next two columns give the amount by which the gas fractions or stellar masses were shifted when calibrating the model. The last column indicates whether the model was run with the fiducial (thermal isotropic) AGN model or with the collimated jet implementation. The last three columns are the three parameters used as input to our baryon response emulator.

Simulation name	fgas $\pm N\sigma$	$M_* \pm N\sigma$	Jet fraction
fgas+2 σ	+2	0	0%
L1_m9 (fgas+0 σ)	0	0	0%
fgas-2 σ	-2	0	0%
fgas-4 σ	-4	0	0%
fgas-8 σ	-8	0	0%
$M_* - \sigma$	-4	-1	0%
$M_* - \sigma$ fgas-4 σ	-4	-1	0%
Jets	0	0	100%
Jets fgas-4 σ	-4	0	100%

2.2 Measurements of power-spectra and baryonic response

The measurement of power spectra is performed over the course of the simulation at 122 different times between $z = 30$ and $z = 0$. At $z < 2$, we obtain a power spectrum measurement after every redshift interval $\Delta z = 0.05$.

For each computation, we deposit the particles on a regular grid of size 256^3 using a triangular-shaped-clouds approach which is self-consistently compensated in Fourier space (see e.g. Jing 2005). Once the density field is computed, we compute its power spectrum using a fast-Fourier transform. To reach k -modes beyond the spacing of the base grid, we use the foldings technique of Jenkins et al. (1998) with a folding factor of 4 between iterations and use 7 iterations. This allows us to measure the matter power spectrum up to scales $k > 1000 h \cdot \text{Mpc}^{-1}$, much beyond the needs of this project.

We measure the total matter power spectrum (i.e. the sum of the gas, dark matter, stars, black holes, and neutrinos) in the hydrodynamical simulations and perform the same computation in the dark-matter-only simulations, where the matter field is represented by a single type of particle. By using the same grid and folding settings between all the runs, we obtain measurements in the same bins in k -space and can thus simply obtain the matter power spectrum ratios, i.e. the baryonic effect on the power spectrum, by dividing the two spectra.

The $z = 0$ baryonic responses for the simulations listed in Table 1 were already presented by Schaye et al. (2023) (their Fig. 22) and compared to the results of the BAHAMAS (McCarthy et al. 2017) and MILLENNIUM-TNG (Pakmor et al. 2023) predictions. Schaye et al. (2023) also showed that the results of the various FLAMINGO runs are in excellent agreement with the model of van Daalen et al. (2020) relating the baryonic response to the mean baryon fraction in clusters of mass $M_{500,c} = 10^{14} M_\odot$, where $M_{500,c}$ is the mass within a radius enclosing a spherical overdensity 500 times larger than the critical density of the Universe.

2.3 Convergence test with simulation volume

As the effect of baryon physics on the matter power spectrum is thought to be driven by haloes of different masses for the different k modes (see e.g. Semboloni et al. 2011; van Daalen et al. 2020; Debackere et al. 2020; Mead et al. 2020; Salcido et al. 2023; van Loon

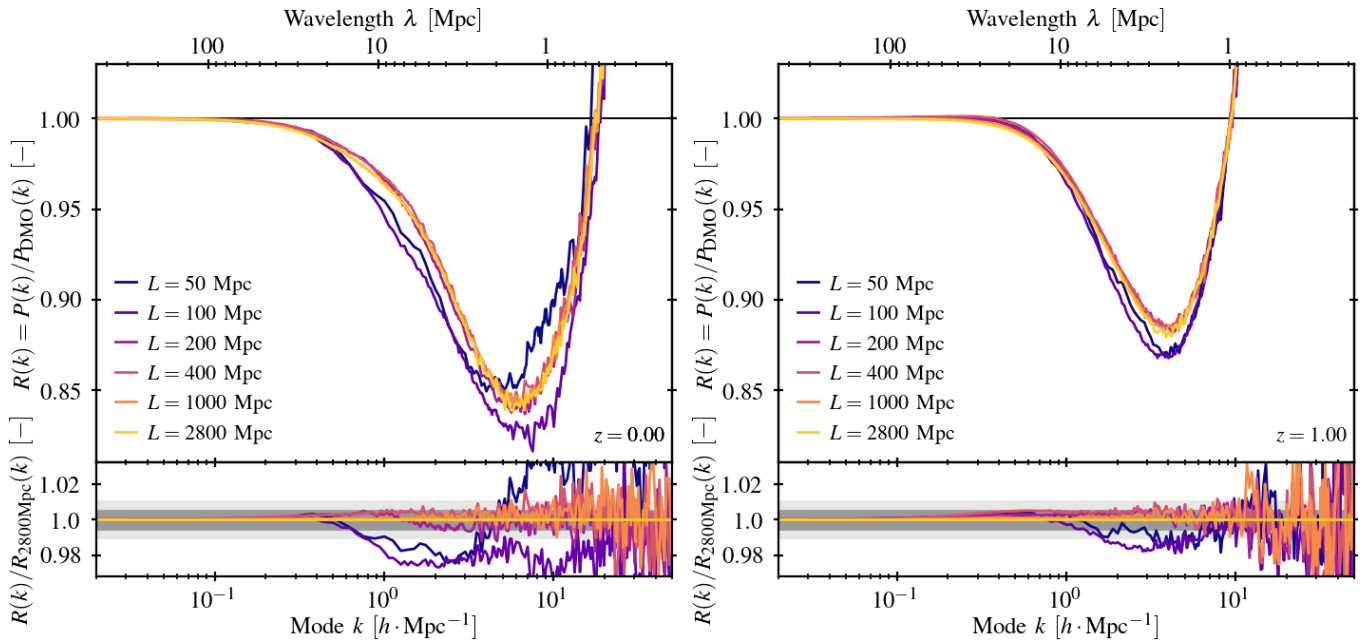


Figure 1. *Top:* The baryonic response at redshift $z = 0$ (left) and $z = 1$ (right) for the fiducial FLAMINGO model extracted from simulations with different volumes, labeled by the box side length. *Bottom:* The ratio of the response in each simulation to the response obtained in the largest simulation ($L = 2800$ Mpc). The shaded regions correspond to fractional errors of 0.5% and 1% respectively. At both redshifts, the results are converged at the 1% level for simulations with volumes in excess of 200^3 Mpc^3 up to $k \approx 10 \text{ h} \cdot \text{Mpc}^{-1}$. Simulations with a side-length of 400 Mpc are not converged to better than 0.5% even on scales $k \approx 1 \text{ h} \cdot \text{Mpc}^{-1}$, with a larger deviation at higher redshift. Note also the reduction in the level of noise when larger simulation volumes are used.

& van Daalen 2024), it is important to ensure that the haloes responsible are well sampled in the simulation volume used for the analysis and are not affected by cosmic variance. To verify this, we present the baryonic response of the matter power spectrum at $z = 0$ and $z = 1$ for different simulations in the FLAMINGO suite using exactly the same galaxy formation model and at fixed resolution in Fig. 1. We use the fiducial FLAMINGO model here (*i.e.* fgas+0 σ , $M^* + 0\sigma$, 0% jet, labeled as the L1_m9 model in Table 1) but we verified that the results are similar for other models. The different line colours correspond to simulations using cubic volumes whose side-lengths are indicated in the figure and range from 50 Mpc to 2.8 Gpc (the ‘L2p8_m9’ model of Schaye et al. 2023).

For volumes with side-length in excess of 200 Mpc at $z = 0$, we find that the baryonic response is converged at the 2% level for the entire range of k values probed by current and upcoming surveys. A convergence to better than 0.5% is only achieved for the simulation with a 1 Gpc side-length. At $z = 1$ (right panel), the convergence at the 1% level is also achieved for volumes $> 200^3 \text{ Mpc}^3$. However, at a more precise level, the simulations are further from the converged result on larger scales than at $z = 0$. As smaller k values are affected by haloes of larger masses, this difference in convergence can be interpreted as the absence of the rarer objects at higher redshift. In the analysis that follows, we will make use of simulations with a volume of 1 Gpc^3 , well within the regime where the results are converged.

Based on this simulation volume analysis, we caution that matter power spectrum responses extracted from simulations such as ILLUSTRIS (Vogelsberger et al. 2014), EAGLE (Schaye et al. 2015), HORIZON-AGN (Chisari et al. 2018), SIMBA (Davé et al. 2019), and CAMELS (Delgado et al. 2023) (all using simulated volumes $\lesssim 100^3 \text{ Mpc}^3$) are likely not converged. Furthermore, if the difference from a converged result in these models has the same sign as we find in the FLAMINGO runs, one could expect the results of these studies to have *overestimated* the baryonic response of these models at $k < 4 \text{ h} \cdot \text{Mpc}^{-1}$. On the other hand, from our analysis the response

reported for the TNG model (Springel et al. 2018) would be converged for their largest volume ($\approx 300^3 \text{ Mpc}^3$). This is confirmed by the results of the MILLENNIUM-TNG simulations, using a very similar model in a 740^3 Mpc^3 volume, reported by Pakmor et al. (2023). We note that if the baryonic response is dominated by the activity in haloes of lower mass than in FLAMINGO (as in e.g. EAGLE or TNG), the response might be converged in smaller volumes already as the number density of the haloes responsible will be less affected by cosmic variance than for our model.

The results of our convergence tests here are consistent with the findings of van Daalen et al. (2011) who found that the total matter power spectra at $z = 0$ are not converged in hydrodynamical simulations with volumes $< (100/h \text{ Mpc})^3$ (their appendix A) and of van Daalen et al. (2020) who found the response to be converged only for volumes $\gtrsim (100/h \text{ Mpc})^3$ (their Appendix A).

3 GAUSSIAN PROCESS EMULATOR

In this section, we describe the procedure used to construct our power spectrum response emulator (§3.1) and the validation steps we performed to assess its quality (§3.2).

3.1 Construction of the emulator

To construct our emulator, we make use of the nine runs listed in Table 1 and measure the baryonic response as described in §2.2. We measure the ratio $R(k) = P(k)/P_{\text{DM0}}(k)$ for 31 values of k logarithmically spaced between $10^{-1.5}$ and $10^{1.5} \text{ h} \cdot \text{Mpc}^{-1}$ (*i.e.* $\Delta \log_{10} k = 0.1$) at five different redshifts ($z = 0., 0.5, 1.0, 1.5,$ and 2.0). We thus have a coarse representation of R as a function of five input numbers: k , z , and the three model parameters used to describe the baryonic physics in the simulations (fgas $\pm N\sigma$, $M^* \pm N\sigma$, and jet fraction) as given in Table 1. Note that even though our simulations are with

the fiducial AGN model *or* the jet-based AGN model, we treat the AGN model as a continuous number going from 0% jet to 100% jet. Similarly, we do not restrict the emulator to only accept input parameter values within the range where it was trained. Whilst these are somewhat uncertain interpolations and extrapolations, we prefer to be able to cover a wide range of scenarios with our model, even if some of them may not be reproduced by actual simulations.

We then train the Gaussian process emulator (see [Rasmussen & Williams \(2006\)](#) for an introduction) provided by the publicly available python package SWIFTEMULATOR² ([Kugel & Borrow 2022](#)), itself an overlay, specialised in scaling relations extracted from simulations, of the commonly used GEORGE³ package ([Ambikasaran et al. 2015](#)).

The emulator was trained on a small number of k bins to reduce the amount of internal data generated and speed up the prediction process. As we will show below, the number of bins we used is sufficient to achieve better than 1% relative accuracy for the range of input parameters relevant to our application. We note that we just used the tools above as-is and that no specific hyper-parameter tuning was necessary. The only hyper-parameter choice made was to force the emulator to assume a mean model of $R(k) = 1 \forall k$ and emulate the difference from this imposed model rather than letting the emulator freely choose a mean $R(k)$ (typically a polynomial) around which to emulate differences.

When using the emulator to make predictions, we use the quadruplet (z , $f_{\text{gas}} \pm N\sigma$, $M_* \pm N\sigma$, f_{jet}) to get the values of R at the 31 points along the k -axis defined above. We then use spline interpolation to compute R at the exact k values of interest. By predicting the value of R for all the 31 k -bins at the same time, we can more rapidly return $R(k)$ for a range of k values at once, which is the most common scenario. As we empirically have $R(k) = 1$ for all $k < 10^{-1.5} h \cdot \text{Mpc}^{-1}$ in our models, we extend our emulator to simply return $R = 1$ on all scales larger than the training range. This effectively allows us to predict the baryonic response in the range $k \in (-\infty, 10^{1.5}] h \cdot \text{Mpc}^{-1}$, meaning that our emulator can easily be coupled to other tools predicting $P_{\text{DMO}}(k)$ to obtain a $P(k)$ including baryon effects over the whole range of scales relevant to current cosmological analysis needs.

We note that the entire prediction step described above takes ≈ 1 ms to be performed on a single compute core. This implies that our emulator can be used in cosmology model inference searches (e.g. using an MCMC sampler) without leading to problematic time overheads. It could also be used as a simple extension to the commonly used Boltzmann solvers such as CAMB ([Lewis et al. 2000](#)) or CLASS ([Lesgourgues 2011](#)) on top of their already-implemented non-linear extensions such as HALOFIT (e.g. [Smith et al. 2003](#)).

The emulator can also optionally return an estimate of the variance for its predictions (See Sec. II.A of [Ambikasaran et al. \(2015\)](#) for the exact definition). This can be useful to estimate the confidence of the emulator in a given part of the parameter space. As we will show below, this variance is overestimated for low values of k as we did not attempt to force the emulator to always return $R = 1$ at values of k close to our largest scale bins.

Our emulator is distributed publicly in the form of a python package named FLAMINGOBARYONRESPONSEEMULATOR and

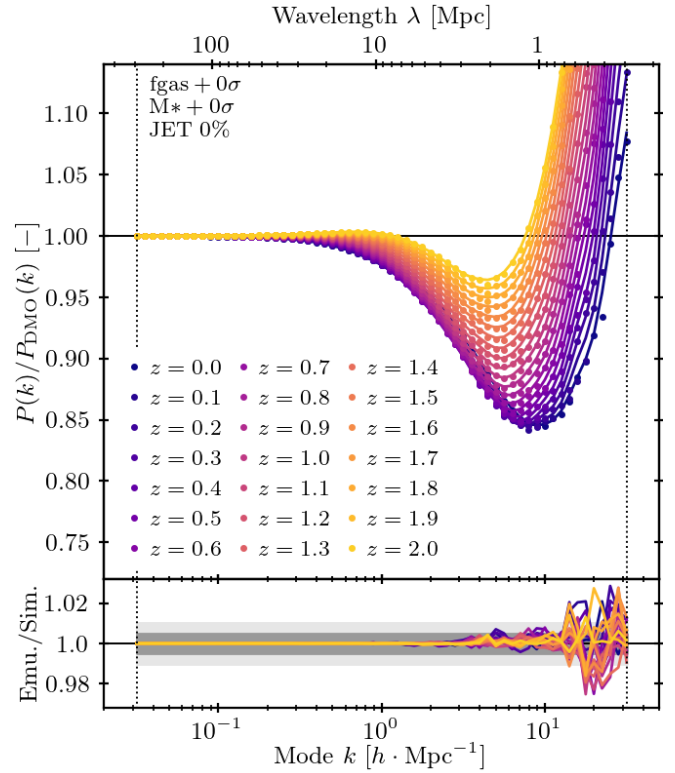


Figure 2. The accuracy of the baryonic response emulator for the FLAMINGO fiducial model (L1_m9) as a function of redshift. The coloured dots show the raw power spectra ratios measured directly from the simulations at 21 different redshifts. The lines show the emulator predictions for the corresponding redshifts. Note that the emulator was only trained on data at an interval $\Delta z = 0.5$. The vertical dotted lines indicate the k -range over which the emulator was trained. The bottom panel shows the ratio between the emulator prediction and the raw simulation output. The shaded regions correspond to fractional errors of 0.5% and 1% respectively. For all redshifts and for all $k < 10 h \cdot \text{Mpc}^{-1}$, the emulator is accurate to better than 1%.

will be made available on the FLAMINGO project web-page⁴ or directly via the `PyPi` package index upon acceptance of this manuscript for publication. Comprehensive documentation and usage examples are provided on the web-page.

3.2 Verification and accuracy

Before exploring the results, we start by assessing the quality of the emulator’s predictions for the data points it was trained on.

In Fig. 2, we show the baryon response for our fiducial model ($f_{\text{gas}} = 0\sigma$, $M_* = 0\sigma$, $f_{\text{jet}} = 0$) at 21 different redshifts and for 61 different values of k . Recall that we only trained on 5 redshifts and 31 bins in k . For each redshift, the dots indicate the raw results from the simulation whilst the lines show the predictions of the emulator. In the bottom panel, we present the ratio between the raw simulation results and the emulator predictions, with the grey shaded regions indicating 0.5% and 1% differences respectively.

Before discussing the performance of the emulator, we analyse the evolution with redshift of the response. We find that the response becomes stronger as the simulation evolves. The position of the minimum of the response moves from $k = 6 h \cdot \text{Mpc}^{-1}$ at $z = 2$ to $k = 10 h \cdot \text{Mpc}^{-1}$ at $z = 0$. The range of scales affected by baryons also

² <https://swiftemulator.readthedocs.io/>

³ <https://george.readthedocs.io/>

⁴ <https://flamingo.strw.leidenuniv.nl/>

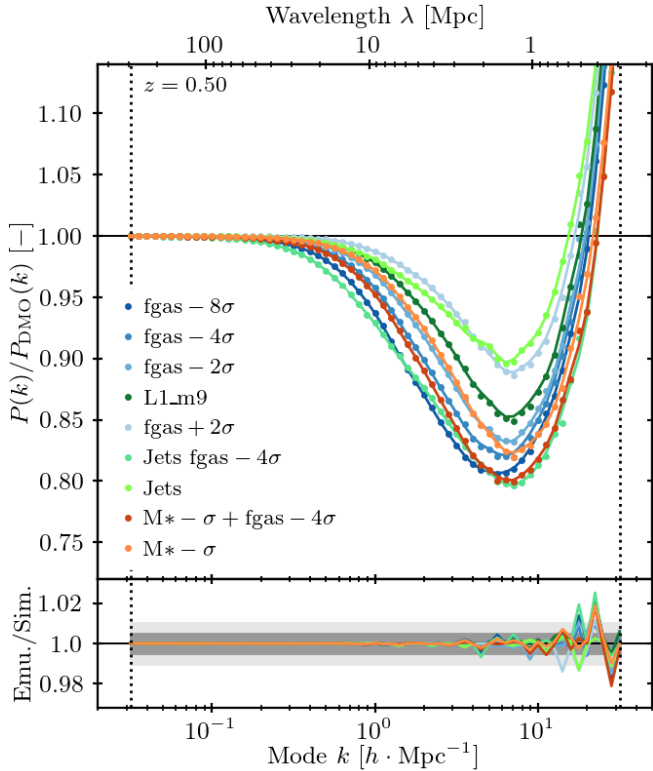


Figure 3. The accuracy of the baryonic response emulator for the FLAMINGO feedback variations (the runs listed in Table 1 with the line colours matching the convention of Schaye et al. (2023)) it was trained on at $z = 0.5$. The coloured dots show the raw power spectra ratios measured directly from the simulations. The lines show the emulator predictions for the corresponding model. The vertical dotted lines indicate the k -range over which the emulator was trained. The bottom panel shows the ratio between the emulator prediction and the raw simulation output. The shaded regions correspond to fractional errors of 0.5% and 1% respectively. For all the models and for all $k < 10 h \cdot \text{Mpc}^{-1}$, the emulator is accurate to better than 1%.

increases with decreasing redshift. At $z = 2$, the response is negligible up to scales $k \approx 1 h \cdot \text{Mpc}$, with the departure from unity (i.e. no response) shifting to $k \approx 0.1 h \cdot \text{Mpc}$ by $z = 0$

Turning now to the verification of our model, we find that for all redshifts shown and for all $k < 10 h \cdot \text{Mpc}$, the emulator described above can reproduce the simulation data with an accuracy better than 1%. At larger values of k , we find that the emulator is less accurate but still returns an answer with a relative error better than 2%.

In Fig. 3, we show the performance of the emulator for the other models it was trained on. We arbitrarily picked $z = 0.5$ for the figure but verified that the results are identical at other redshifts. The conclusion here is similar to the one for the previous exercise: the emulator reaches a relative accuracy better than 1% for $k < 10 h \cdot \text{Mpc}$ and degrades to around 2% on smaller scales.

To be more quantitative, we measured the relative difference between the emulator predictions and the raw simulation results for all $z < 2$ at which we have data and for all nine feedback models. We recorded the maximal error reached and found that at $k < 10 h \cdot \text{Mpc}$, this never exceeds 1.1%. At $k < 3 h \cdot \text{Mpc}$ and for $0 \leq z \leq 2$, the most relevant range for current cosmology measurements, the relative error of the emulator is always smaller than 0.25%.

We can thus conclude that the emulator designed in the previous section faithfully reproduces the raw simulation results. Unless stated otherwise, the rest of this paper will only use the emulator to show results and not the raw simulation data.

3.3 Alternative description of input parameters

As discussed in § 2.1 and more thoroughly in Kugel et al. (2023), the FLAMINGO simulations were calibrated to match the inferred gas fractions from a combined data set of X-ray and weak-lensing. We then uniformly shifted the data by a certain number of σ and calibrated the model to match these shifted data sets. The ‘fgas $\pm N\sigma$ ’ input parameter of our emulator corresponds to the σ -shift with respect to the original data set used by Kugel et al. (2023). Instead of referring to models defined with respect to a fixed data set, it may be advantageous to instead use the absolute gas fractions in groups or clusters as the input parameter of the emulator.

van Daalen et al. (2020) showed that across many galaxy formation models, a tight relationship exists between the baryon fraction in a certain halo mass bin and the baryonic response at a fixed scale k . Different halo masses then dominate the effect at different k values (see also van Loon & van Daalen 2024). Using these fractions is thus a meaningful input parameter that can also be directly related to observables. Similarly, the response emulator from the ANTILLES suite (Salcido et al. 2023) also uses the baryon fraction (either at a fixed halo mass or across a range of masses) as input to their model. However, given the limited range of models varying the stellar fractions in the FLAMINGO suite, we choose to instead use the gas fractions as the parameter we vary and leave the exploration of more general variations where we alter both the stellar and gas fractions (and thus the baryon fractions) to a future study.

As various observational data sets are able to constrain the gas fractions in different halo masses and because the FLAMINGO simulations may not necessarily match the trend with mass of all these observations, we decided not to pre-define a specific halo mass for which the gas fraction is used as input to our model. We, instead, choose to present the connection between the gas fraction at $z = 0$ and the actual input parameter ‘fgas $\pm N\sigma$ ’ in Fig. 4 and let users of our package decide based on their available observational input data which halo mass best suits their needs.

In Fig. 4, we show, using different line colours for each halo mass, the mapping between the gas fractions in the simulation at that halo mass and the input parameter ‘fgas $\pm N\sigma$ ’ of our emulator. We use $M_{500,c}$ as our halo mass definition and report the gas fractions (normalised by the cosmic mean) within the corresponding over-density radius $R_{500,c}$. This choice was made to match the radii commonly used by cluster studies. The dashed lines correspond to the simulations using the jet AGN implementation. Note that since this model was only run for two different values of ‘fgas $\pm N\sigma$ ’, the mapping at more extreme values is not available.

For intermediate masses, $M_{500,cr} \sim 10^{14} M_{\odot}$, the two models for AGN feedback agree (i.e. the solid and dashed lines overlap). This is largely a consequence of the calibration effort as this is the mass range that was the most constraining in the data set used by Kugel et al. (2023). At higher, and especially at lower masses, the two models start to differ. This, in turn, leads to differences in the baryonic response these models generate for a fixed ‘fgas $\pm N\sigma$ ’, as can be seen in Fig. 3 when comparing the ‘Jets’ and ‘L1_m9’ models (both using ‘fgas=0 σ ’) or the two models calibrated to ‘fgas=−4 σ ’.

One can then use Fig. 4 and the gas fractions obtained from observed data sets to set a prior on the range of values our parameter ‘fgas $\pm N\sigma$ ’ can take; for instance when attempting to marginalize over baryon effects for cosmology inference.

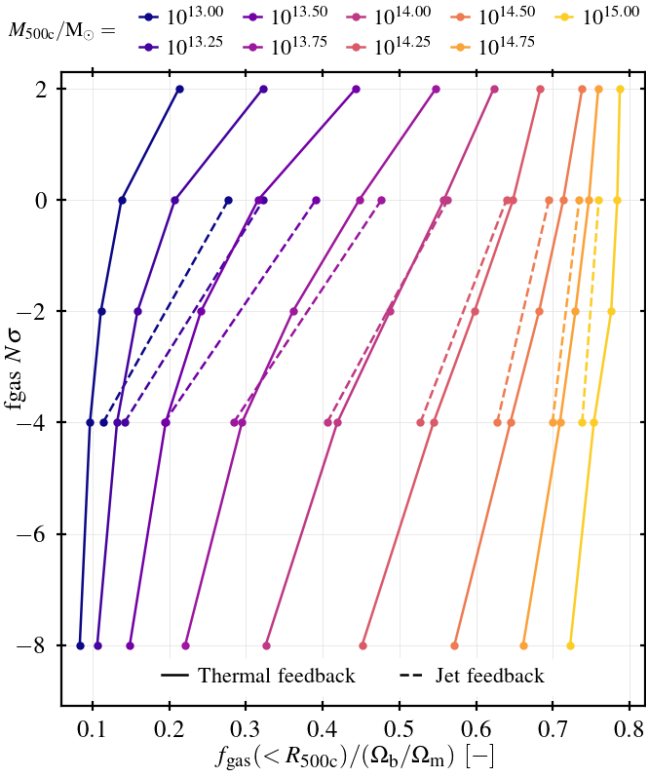


Figure 4. The value of the $f_{\text{gas}} \pm N\sigma$ input parameter to our emulator as a function of the $z = 0$ gas fraction within $R_{500,\text{cr}}$ of the simulated clusters for different halo masses (different line colours). The solid lines correspond to the values extracted from the simulations with the thermal AGN model whilst the dashed lines show the values for the simulations exploiting the jet-based AGN model.

4 RESULTS

Having demonstrated that the emulator we built is sufficiently accurate, we now turn to the exploration of some of the baryonic response predictions of the FLAMINGO model.

4.1 The baryonic response in FLAMINGO

In this section, we present a selection of results at $z = 0$ by varying the emulator’s input parameters one by one.

4.1.1 Varying the gas fraction for the thermal AGN model

We start by studying the effect of changing the ‘ $f_{\text{gas}} \pm N\sigma$ ’ parameter for the purely thermal AGN model while keeping the stellar masses at their fiducial values. In Fig. 5, we vary this parameter from -10 to $+4$, *i.e.* going from a model that would lead to gas fractions in clusters 10σ below the data used for calibration to a model 4σ above it. The different line colours correspond to the responses for the different parameter values. We use solid lines to indicate models for which we have a simulation and which were thus part of the training set. For these, we additionally show using dots the actual simulation data. The dashed lines correspond to the emulator’s prediction for models where no simulation currently exist and are thus interpolations or extrapolations beyond the training set. Finally, we indicate using a shaded region the $2-\sigma$ error estimate on the prediction reported by the emulator (for a formal definition see Ambikasaran et al. 2015).

As can be seen, the response becomes larger as the value of the

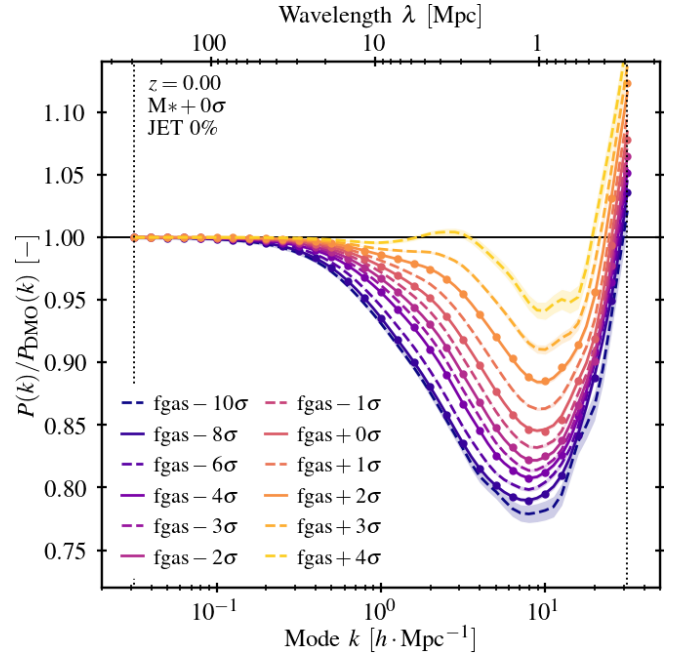


Figure 5. Predictions of the FLAMINGO baryon response emulator at redshift zero for different models using thermal AGN feedback deviating from the X-ray inferred gas fractions the simulations were designed to reproduce and expressed as the number of sigma discrepancy between the calibrated gas fraction and the data. The variables kept fixed in the emulator are displayed on the top left. The dots correspond to raw data from the simulations with the solid lines showing the emulator prediction at the same value of $f_{\text{gas}} \pm N\sigma$. The dashed lines show the emulator predictions for interpolation or extrapolation beyond the simulations used for its construction. The shaded regions show the 2-sigma uncertainty of the emulator prediction.

parameter ‘ $f_{\text{gas}} \pm N\sigma$ ’ decreases. This is, in agreement with previous studies linking the baryon content of clusters to the intensity of the response in simulations (e.g. Semboloni et al. 2011, 2013; van Daalen et al. 2020; Salcido et al. 2023) or from empirical/phenomenological models (e.g. Schneider et al. 2019; Debackere et al. 2020; Aricò et al. 2021; Mead et al. 2021). At values of ‘ $f_{\text{gas}} \pm N\sigma$ ’ below -8 , the change in the response becomes smaller and the predicted response overall reaches a saturation value; meaning the FLAMINGO model cannot produce an even stronger response when only this parameter is changed. We note, however, that we have not run a simulation at that point; this is an extrapolation from the emulator only.

Similarly, at values of the parameter much above the training regime, we find that the predicted response from the emulator flirts with the unity line, in a likely unphysical manner. Whilst understanding the behaviour of the model in this regime could lead to valuable physical insights, we choose not to spend more time in this area as the match to observations and cosmological data sets seems to require a response that is typically stronger than our fiducial model (e.g. McCarthy et al. 2024), let alone models overshooting the gas fraction data we calibrated to.

Note also the position of the minimum of the response. For the values of ‘ $f_{\text{gas}} \pm N\sigma$ ’ explored here, we find that the minimum stays in the range $k = 8$ to $10 h \cdot \text{Mpc}^{-1}$ with a weak dependence on ‘ $f_{\text{gas}} \pm N\sigma$ ’. To first order, the input parameter changes the normalisation of the response without changing the affected range of k . It is instructive to compare this to Fig. 2 where we see that the position of the minimum does decrease systematically with redshift.

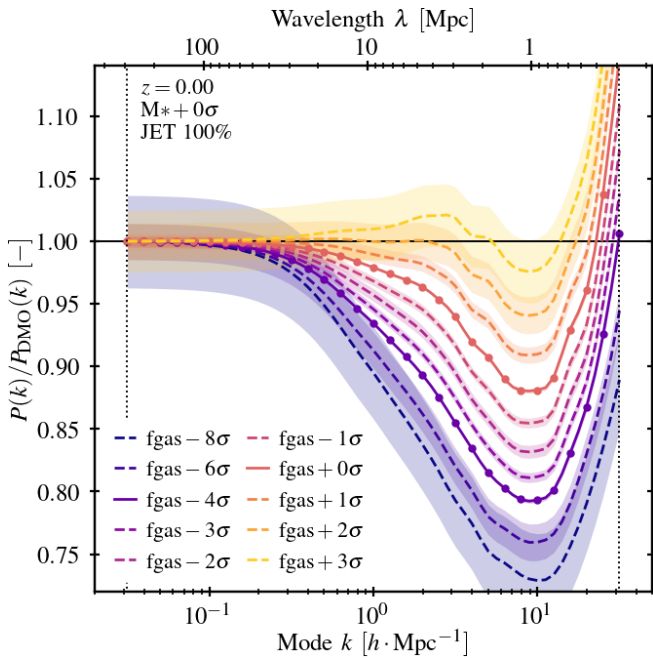


Figure 6. Same as Fig. 5 but for the model using the AGN jet model. For $f_{\text{gas}} \pm N\sigma$ values beyond the training range, the emulator returns a large uncertainty, even at low values of k . The prediction error is there largely overestimated, mainly due to the fact that there are only two simulations sampling this part of the parameter space. At fixed value of $f_{\text{gas}} \pm N\sigma$, the emulator predicts a larger response than in the case with purely thermal AGN.

4.1.2 Varying the gas fraction for the jet AGN model

We now repeat the exercise of varying ‘ $f_{\text{gas}} \pm N\sigma$ ’ but for the model with ‘100% jet’. In terms of the 3D parameter space of inputs to our emulator, we are exploring the same directional vector as above but starting from a position shifted along the jet fraction axis. The result of this exercise is displayed in Fig. 6 where we used the same line style convention as in the previous figure.

As can be seen, the size of the shaded regions indicating the emulator uncertainty is significantly larger than for the thermal AGN model (i.e. 0% jet). This stems from the fact that we have only two runs (the two solid lines in the figure) using the jet AGN model and the predictions made in this area of the parameter space are thus more uncertain, especially when extrapolating beyond the training range. Note also that we do not show the ‘ $f_{\text{gas}} - 10\sigma$ ’ and ‘ $f_{\text{gas}} + 4\sigma$ ’ predictions as their large uncertainties make them lose any significance. The uncertainty at low k is strongly overestimated as all physical models have to return to unity in that regime; at least for the range of parameters explored here. This large uncertainty is a consequence of keeping our emulator simple with no physical insights that would allow it to return a more physically-motivated uncertainty in the low- k regime. It is possible that a different choice of mean model for the emulator would have led to a smaller error estimate. We do, however, prefer to keep the model as shown here; the level of uncertainty that is acceptable will be application-dependent. We thus leave the choice of what to use to users of the emulator.

Overall, the baryonic response obtained for our model with 100% jet shows a stronger dependence on the input parameter value than for the equivalent model with 0% jet. For negative values of ‘ $f_{\text{gas}} N\sigma$ ’, the response is stronger and for positive values it is weaker than in the thermal AGN case. However, the range of the k -range affected and the position of the minimum are similar.

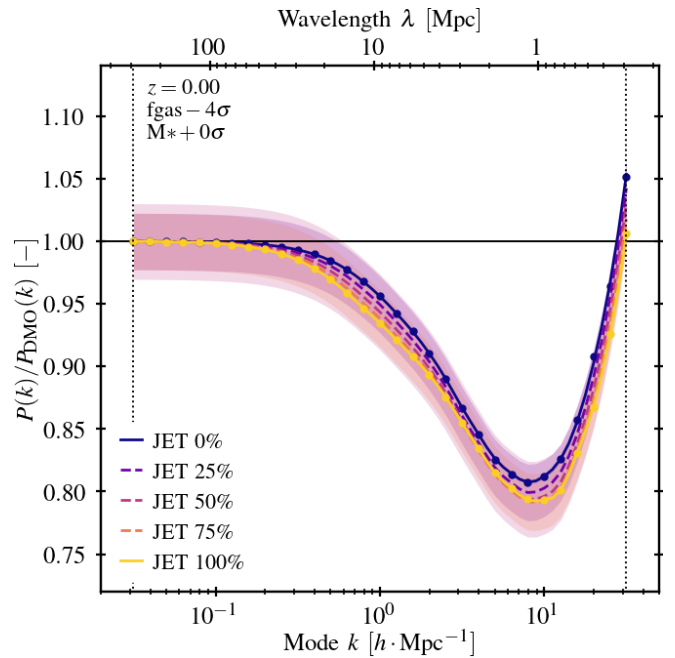


Figure 7. Same as Fig. 5 but for predictions of the FLAMINGO baryon response emulator when the fraction of AGN work done by the jet model is varied between 0% and 100%, here for models fitting the gas fraction data shifted by -4σ . Note that simulations have only been performed at the two extremes of the jet fraction range.

4.1.3 Interpolating between AGN models

The impact of the choice of AGN model is clear from the previous two figures. As we constructed our emulator with the formally binary jet model option replaced by a continuous fraction, we can explore the effect of changing the model. We show this in Fig. 7, where we vary the jet fraction for the case of ‘ $f_{\text{gas}} - 4\sigma$ ’. We picked this value of the gas fractions for the figure as it shows a larger difference between models than for the fiducial ‘ $f_{\text{gas}} + 0\sigma$ ’ but the effect is similar at other values. We note that there is no simple way to generate an actual FLAMINGO simulation that has a jet fraction other than 0% or 100%. The results shown here are purely an interpolation constructed from the emulation.

As can be seen from the figure, the response is stronger for a larger jet fraction. This is consistent with the gas fractions shown in Fig. 4, with the halo masses, at the relevant k -scale, most responsible for the response displaying a lower gas fraction in the jet model (dashed lines). The uncertainty reported by the emulator is here again quite large, largely because only two actual simulations span this dimension of the training set. The uncertainty at low- k is also likely overestimated given that all models are expected to return to unity there.

4.1.4 Varying the stellar fractions in the model

Having explored the first two dimensions of the parameter cube, we now turn to the variation of the last input parameter, the change in the $z = 0$ stellar masses. This corresponds to models where the mass of every galaxy is lowered/increased by a certain number of σ from the original data (GAMA DR4, Driver et al. 2022) that the fiducial FLAMINGO simulations were calibrated to. We show the effect of this parameter in Fig. 8, where we adopt the same line style convention as for the three last figures. Along this axis, the number of actual training points is again very small (two) so the emulator’s predictions become rapidly very uncertain. The uncertainty on the ob-

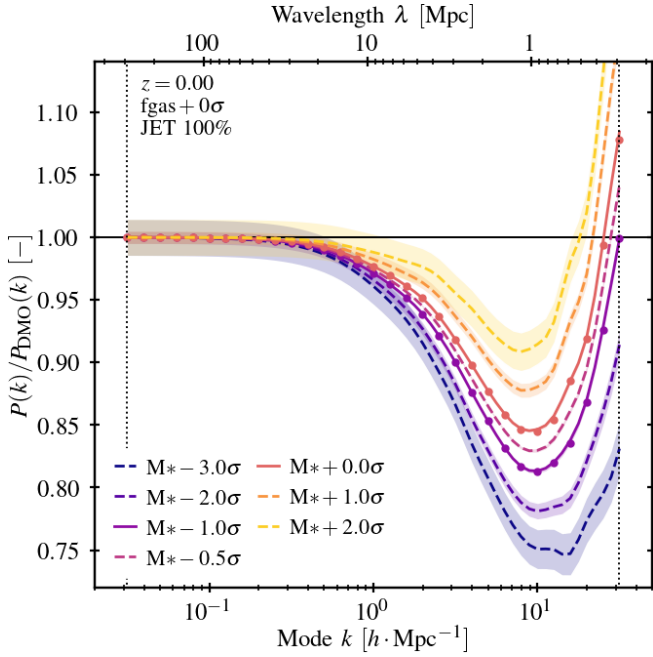


Figure 8. Same as Fig. 5 but varying the fit to the $z = 0$ stellar mass function whilst keeping the gas fraction in clusters fixed to the fiducial value.

served data is, however, much smaller here than for gas fractions and this does leave us with less freedom to drastically change the amount of stellar mass formed overall in our simulations. The effect of this parameter is smaller than the changes in the gas fractions studied above. The uncertainty on the stellar masses in the data only significantly impacts the baryonic response for $k > 1 h \cdot \text{Mpc}^{-1}$. At fixed gas fraction in clusters, we find that a lower stellar mass function leads to stronger baryonic response. This is in line with expectations as it requires the stars and the AGN to provide more feedback to suppress the formation of stars in the objects on top of the feedback required to obtain the requested gas fraction.

As discussed in § 3.3, a future improvement of our emulator will be to offer more variations of both the gas *and* stellar fractions independently to have a broader coverage of the possible baryon fraction in clusters, akin to the model of Salcido et al. (2023). We leave these improvements for a future release of more FLAMINGO simulations extending the parameter space in these directions.

4.2 Evolution with redshift

In the previous subsection, we focused on the results at $z = 0$. As most of the cosmology surveys use data at higher redshifts and using many bins or bins spanning a wide redshift range, it is interesting to quantify the evolution of the response with redshift. Our emulator was trained with data from the simulations up to $z = 2$, a range beyond sufficient for all current and upcoming surveys. It can thus be directly used in the analysis of survey data.

The evolution of the response, in particular of the k -range affected and of the position of the minimum of the response, with redshift for our fiducial model was already presented in Fig. 2. Besides this base case, exploring the full range of models discussed in § 4.1 across all redshifts would extend our study too much, we thus restrict our evolution analysis here to the simple question of whether models with stronger feedback also display a stronger evolution in time. To measure this, we take the baryonic response at $z = 1$ and compare it to the response at $z = 0$ for different values of the “fgas” parameter. The

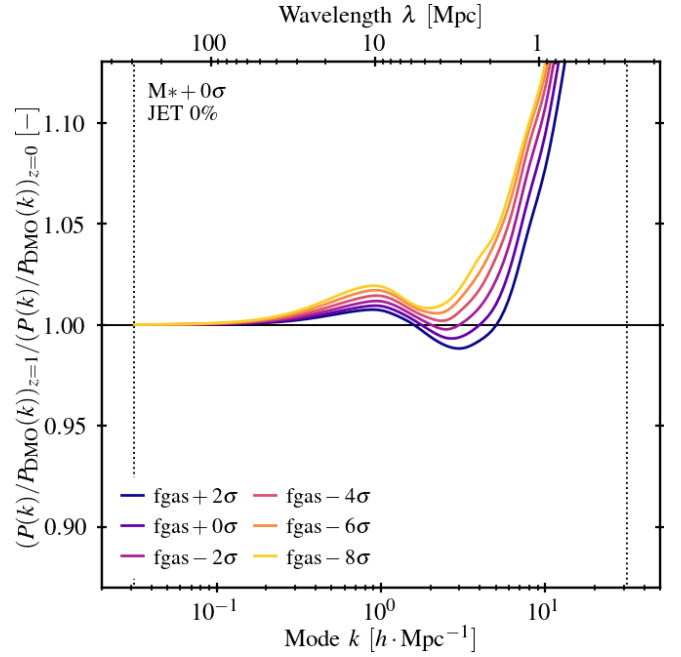


Figure 9. The ratio of the baryonic response at redshift $z = 1$ and $z = 0$ for models with different values of the $\text{fgas} \pm N\sigma$ value, as indicated in the legend. Note the smaller range of the vertical axis used here. Models with no redshift evolution of the response would display a flat line on this figure. The models with lower gas fractions in clusters, i.e. with more intense feedback, show a stronger evolution with redshift of the predicted baryonic response.

result of this experiment is displayed in Fig. 9 where we show the ratio between the two responses. The different coloured lines correspond to different values of “fgas” (i.e. different feedback strengths). Models displaying no evolution in their response between $z = 1$ and 0 would be shown as a horizontal line of value 1. The further a model is from this line (in either direction), the more redshift evolution is found. As can be expected, the stronger the feedback response at $z = 0$ (i.e. the smaller the value of “fgas”), the stronger the evolution. The responses for different feedback strengths thus look more similar at higher redshift. As the response is mainly driven by the AGN-induced gas flows in large haloes (e.g. van Daalen et al. 2011), we can qualitatively understand this trend by the need of massive galaxies to first form and by the time it then takes for the expelled gas to reach large distances.

We note that we have verified that the same trend holds for models using a jet fraction > 0 or a different $M^* - \sigma$ value.

4.3 Dependence on the cosmological model

The emulator was trained on simulations that all assume the same background cosmology. If the emulator is to be used in cosmology inference using survey data, this would imply that we *assume* that the response is independent of the cosmology chosen. Whilst verifying this assumption is a critical task, it is beyond the scope of this paper and of the current range of simulations present in the FLAMINGO suite.

Elbers et al. (2024) explored the correlation between cosmological model and baryonic response in the FLAMINGO simulations, especially in the context of neutrino mass variations. They found a small dependence, which they were able to explain using the changes in the halo mass-concentration relation induced by the changes in the cosmology. We do not repeat this exercise here, but we complement it with an analysis of an additional two simulations

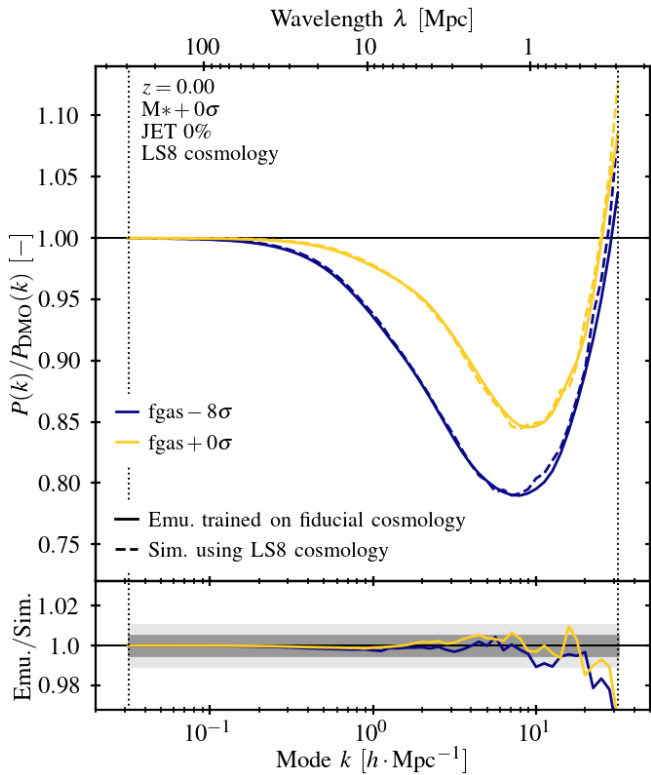


Figure 10. Comparison of the matter power spectrum baryonic response from our emulator (solid line) trained on our runs using our fiducial cosmology to the responses obtained from simulations using our low S_8 (LS8) cosmology (dashed lines). The bottom panel shows the ratio of the prediction of the emulator, trained on our fiducial cosmology model only, to the two simulations we have run using the LS8 cosmology. The shaded regions indicate $< 0.5\%$ and $< 1\%$ relative difference with respect to the raw simulation prediction. For the relevant range of k -scales and for the two models which span a wide range of possible responses within the FLAMINGO suite, we find that the cosmology dependence of the baryonic response is below 1% of the total signal.

using the “lensing cosmology” (LS8) cosmological model ($\Omega_m = 0.305$, $\Omega_b = 0.0473$, $\sigma_8 = 0.760$, $h = 0.682$, $n_s = 0.965$, $\sum m_\nu c^2 = 0.06$ eV) of [Amon & Efstathiou \(2022\)](#). We ran two simulations with this background cosmology. The first one using the “fgas+0 σ ” baryon physics model and the second one using the “fgas-8 σ ” one. These two models largely bracket the responses we obtained in the FLAMINGO suite. We then compare the baryonic responses predicted by these simulations to the predictions of the emulator that was trained on the fiducial cosmology.

We show this comparison in Fig. 10. The emulator predictions are shown as solid lines whilst the raw simulation data is displayed using dashed lines. The bottom panel shows the ratio between the two to highlight the differences. For both feedback models (different colours), we find that the relative difference between the emulator predictions (trained on our fiducial cosmology) and the raw simulation data is smaller than 1% for all $k < 10 h \cdot \text{Mpc}^{-1}$. The figure shows this comparison at $z = 0$ but we verified that the same conclusion holds also at higher z .

Interpreting this result in the light of the analytic model of [Elbers et al. \(2024\)](#), we can understand the small difference due to cosmology as coming from the small change in the mass-concentration relation of haloes between our fiducial cosmology and the LS8 one (as expected from models of the concentration such as [Correa et al. 2015](#)). From the analysis of [Elbers et al. \(2024\)](#), we do expect to

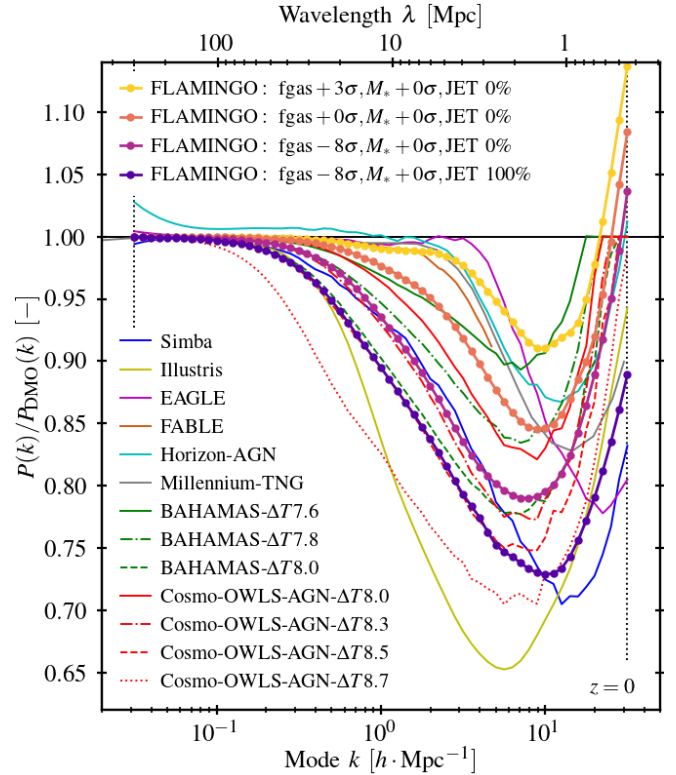


Figure 11. Comparison of the $z = 0$ matter power spectrum baryonic response in four FLAMINGO models (from our emulator) to the response obtained in a selection of simulations from the literature (see text for details). Depending on the input parameters, the response returned by the FLAMINGO emulator can be similar to many published models; only the models with the strongest feedback are beyond the range of our emulator. Of particular interest are the two models at “fgas-8 σ ” using the thermal and jet models which closely resemble the COSMO-OWLS models with $\Delta T_{\text{AGN}} = 8.3$ and 8.5 respectively that are often used in the literature as representatives of the baryonic response in hydrodynamical simulations.

find larger differences (up to a few percent at $k = 10 h \cdot \text{Mpc}^{-1}$) for variations within ΛCDM that affect the mass-concentration relation more (see their section 4).

We leave the full exploration of the cosmological dependence of the power spectrum response to a future study, where we will expand the emulator to also predict the response as a function of cosmological parameters.

4.4 Comparison to other studies

We conclude our description of the baryonic response in FLAMINGO with a comparison of our model to results from other simulations and models. We restrict our analysis to $z = 0$ but understanding the evolution of the response with time will be important for current and future surveys where data from a wide range of redshifts enters the analysis.

4.4.1 Comparison to hydrodynamical simulations

In Fig. 11 we compare four models extracted from our emulator to a selection of simulations from the literature. We use here the compilation of homogenized data from [van Daalen et al. \(2020\)](#), expanded to more recent runs. In particular, we show the results from SIMBA ([Davé et al. 2019](#)), ILLUSTRIS ([Vogelsberger et al. 2014](#)), EAGLE

(Schaye et al. 2015), FABLE (Henden et al. 2018), HORIZON-AGN (Chisari et al. 2018), MILLENNIUM-TNG (Pakmor et al. 2023), three variations of BAHAMAS (McCarthy et al. 2017), and four variations of COSMO-OWLS (Le Brun et al. 2014). Note that, as discussed in § 2.3, some of these simulations exploited volumes that are likely too small to produce converged results.

As can be seen, the range of predictions from all these models is relatively broad, as is the baryon fraction in clusters they predict (van Daalen et al. 2020). Nevertheless, our emulator can cover a large range of models with its predictions. Only the two most extreme models (ILLUSTRIS and COSMO-OWLS-AGN- $\Delta T_{\text{AGN}}=8.7$) are beyond the reach of our emulator, and likely of what the FLAMINGO family of simulations can produce without alterations to the physics.

It is interesting to note that our models with “fgas-8 σ ” using the thermal and jet models closely resemble the COSMO-OWLS models with $\Delta T_{\text{AGN}} = 8.3$ and 8.5 respectively. The latter of these two models is often used as a representative of a large baryonic response when analysing data sets (e.g. Mead et al. 2020; Amon & Efstathiou 2022; Preston et al. 2023; Bigwood et al. 2024). Fine tuning of the parameters of the emulator could likely lead to our model matching other simulations shown here. We thus conclude that our family of models and the emulator constructed on top of it are able to cover almost the entire range of predictions from the literature. Missing the strongest responses is, however, possibly a limitation as recent studies seem to suggest stronger responses are required to explain the data (Amon & Efstathiou 2022; Preston et al. 2023), in particular kSZ observations (Bigwood et al. 2024; Hadzhiyska et al. 2024; McCarthy et al. 2024) and the tSZ power spectrum (McCarthy et al. 2014, 2018, 2023).

With its connection to gas fractions at specific halo masses (Fig. 4), our emulator can be meaningfully be related to observables. These can in turn be used to provide a prior on the range of responses compatible with the data. The more meaningful labelling of the models via “fgas $\pm N\sigma$ ”, as compared to a label based on subgrid parameter values, helps in this respect.

4.4.2 Comparison to the ANTILLES suite

Using the ANTILLES suite of 400 simulations run with the OWLS model, Salcido et al. (2023) constructed a model, “SP(k)”, predicting the baryonic response using the baryon fraction in groups and clusters as input parameter to their model. Their much wider range of simulations allows them to encompass a much wider range of possible responses than we can with our FLAMINGO-based emulator. They offer multiple versions ranging in complexity of the input going from a single parameter to providing the fractions over a range of halo masses. We use this latter version here to compare to our models. Specifically, we measured the baryon fractions as a function of halo mass (note the difference with the gas fractions we used in Fig. 4) for our fiducial FLAMINGO model and used them as an input to their model. The resulting response is shown for five different redshifts in Fig. 12 alongside the response obtained from our emulator.

As can be seen, despite using the exact baryon fractions of the simulations as input, the SP(k) model predictions do not match the FLAMINGO results. They predict a stronger response at $k \approx 1h \cdot \text{Mpc}^{-1}$ and a weaker one at $k > 3h \cdot \text{Mpc}^{-1}$, in particular at low redshift. This indicates that knowing the baryon fraction in haloes is not a sufficient condition to obtain the baryonic response. Indeed, Debackere et al. (2020) used a halo model to show that the baryon fraction beyond R_{500c} is important.

The FLAMINGO and ANTILLES simulations do not have the same

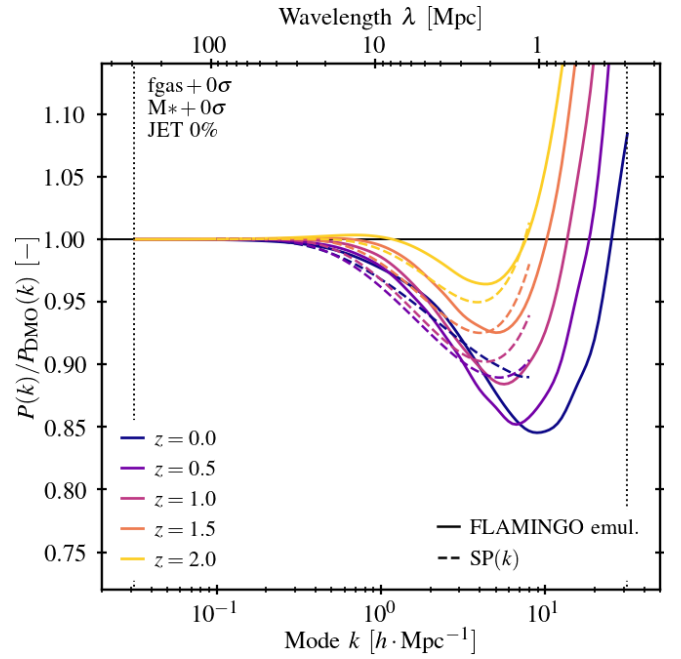


Figure 12. Comparison of the matter power spectrum baryonic response at different redshifts in the fiducial FLAMINGO simulation from our emulator (solid lines) to the one predicted by the SP(k) model of Salcido et al. (2023) (dashed lines) fitted to the true $M_{500,c}$ - baryon fraction relation extracted from the FLAMINGO halo catalogs.

stellar fraction in their haloes and this likely explains part of the difference here. Note that it may be possible to explore our emulator to match SP(k) more closely. One could, for instance, lower “ $M^* \pm N\sigma$ ” whilst increasing “fgas $\pm N\sigma$ ” in order to maintain the same baryon fraction in haloes. However, as we do not have predictions for the stellar fractions as a function of these parameters, we leave this exercise for a future study with a more comprehensive emulator. This simple comparison nevertheless indicates that predicting the baryonic response using a single number (e.g. the baryon or gas fraction) per halo mass bin may not be sufficient and more complex models will have to be constructed in the future.

4.4.3 Can FLAMINGO feedback solve the S_8 tension?

Over the last few years, precision tests of the Λ CDM models, particularly those exploiting low-redshift weak-lensing and large-scale structure probes, have reported measurements of $S_8 \equiv \sigma_8 \sqrt{\Omega_m/0.3}$ in conflict with the value inferred from the primary CMB anisotropies and BAO experiments. Depending on the data sets and their analysis, this so-called tension can reach 3σ (Heymans et al. 2021; Abbott et al. 2022; Amon et al. 2023; Miyatake et al. 2023; McCarthy et al. 2023).

Among the different solutions put forward to solve this tension, the possibility that (baryon and galactic feedback) physics on the scales of groups and clusters contributes to the non-linear effects on the range of scales on which the power spectrum is probed is an interesting proposition as it does not require an alteration of the background cosmological model. We explore here whether the response obtained in the FLAMINGO model is compatible with the required baryon-induced non-linear solution to the tension.

Amon & Efstathiou (2022) constructed a toy model for the effect of baryons, inspired by the functional form obtained from the HM-CODE2020 (Mead et al. 2020), and constrained it to reconcile the weak-lensing shear analysis of the KiDS-1000 survey and the pri-

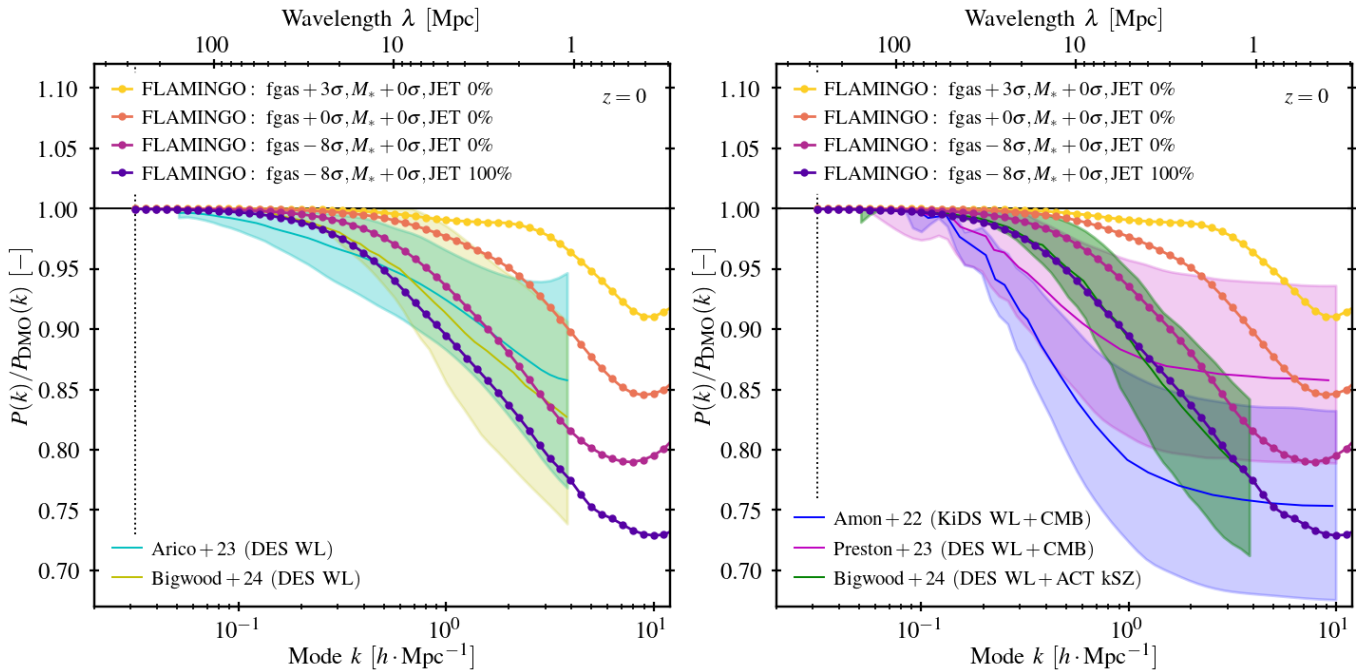


Figure 13. Comparison of the $z = 0$ matter power spectrum baryonic response in four FLAMINGO models (from our emulator) to the response inferred from the analyses of different weak-lensing cosmology probes combined with a halo model or a baryonification model. The right panel shows analyses where in addition either primary CMB anisotropy data or kSZ data was used to infer the response (see text for details). Note the reduced k -range plotted here compared to the previous figures.

mary CMB anisotropy data. Using a similar approach, [Preston et al. \(2023\)](#) combined the DES year 3 shear data to the CMB data to also constrain the required non-linear power spectrum changes. Both these constraints are shown as, respectively, the blue and magenta shaded regions in the right panel of Fig. 13. A parallel approach is to exploit the weak-lensing data alone in combination with a halo model or emulator for the baryonic response. The analysis of [Aricò et al. \(2023\)](#) and [Bigwood et al. \(2024\)](#), both exploiting the DES year 3 data but with different emulators (BACCO ([Aricò et al. 2021](#)) and BCEMU ([Giri & Schneider 2021](#)) respectively) and different analysis pipelines, are shown as shaded regions in the left panel of Fig. 13. Finally, additional datasets informing the emulators or models on the gaseous content of haloes can be used. The constraints of [Bigwood et al. \(2024\)](#) including kSZ data from ACT are shown in the right panel of Fig. 13 (see also [Schneider et al. 2022](#)). In both panels, we show the response obtained for four models spanning the range of FLAMINGO emulator input parameter values.

As can be seen, the more extreme models in the FLAMINGO suite are compatible with some of the inferred baryonic responses in these studies. In particular, both the two ‘ $f_{\text{gas}} - 8\sigma$ ’ models (i.e. with thermal AGN and with collimated jet AGN) are within the ranges demanded by the analysis of [Bigwood et al. \(2024\)](#) (with or without added kSZ constraints). Interestingly, these FLAMINGO models display gas fractions that are in strong tension with the gas fractions in groups and clusters inferred from joint X-ray and weak-lensing analyses ([Kugel et al. 2023](#)). Putting aside the option of systematic error or selection effects affecting either data sets, this could indicate that more complex physics, for instance more advanced feedback models, are required in simulations to jointly match the X-ray and kSZ measurements (see also [Hadzhiyska et al. 2024](#); [McCarthy et al. 2024](#)).

The constraints on the power spectrum response derived by [Amon & Efstathiou \(2022\)](#) and to a lesser extent [Preston et al. \(2023\)](#) and [Aricò et al. \(2023\)](#) (at $k \lesssim 0.5 h \cdot \text{Mpc}^{-1}$) are out of reach of our emu-

lator and likely of what can be achieved using the FLAMINGO model without altering the sub-grid models. If the Universe does look like a FLAMINGO model with extreme feedback (e.g. ‘ $f_{\text{gas}} - 8\sigma$ ’), the tension between the CMB and the low-redshift small-scale probes would nevertheless be reduced, though a more quantitative analysis of this change is left for future studies. Note, however, that the S_8 tension also manifests itself in other probes not related to weak-lensing, such as in the thermal SZ power spectrum (see e.g. [McCarthy et al. 2014, 2018, 2023](#)) and that altering the small-scale matter power spectrum may not be sufficient.

5 CONCLUSIONS

In this study, we used the hydrodynamical simulations from the FLAMINGO project ([Schaye et al. 2023](#); [Kugel et al. 2023](#)) and extracted their total matter power spectra, which were then compared to ones taken from the dark matter only counterparts of the simulations. By taking the ratio of the two matter power spectra, we obtained the baryonic response of the matter power spectrum generated by baryonic physics associated with galaxy formation. We then constructed a Gaussian process emulator using four parameters: the redshift and the three parameters describing baryon physics of the simulations as input parameters to reproduce the simulated baryonic response in the range of scales $k = 10^{-1.5} - 10^{1.5} h \cdot \text{Mpc}^{-1}$, sufficient for all current and planned large-scale structure probes. These parameters are the offset of the gas fractions in clusters with respect to the simulation calibration data (‘ $f_{\text{gas}} \pm N\sigma$ ’), the offset of the galaxy masses used for the calibration (‘ $M_* \pm N\sigma$ ’ and the fraction of AGN feedback output in the form of collimated jets. We then explored the accuracy of the emulator thus constructed and the general predictions for the baryonic response in the FLAMINGO simulations. Our findings can be summarized as follows:

- The baryonic response at $z = 0$ and $z = 1$ is converged to better

than 1% only for simulations using volumes in excess of 200^3 Mpc^3 . A convergence to better than 0.5% is only achieved for volumes larger than 400^3 Mpc^3 and the higher redshift results display a difference with respect to the converged answer on larger k -scales than at lower redshift (Fig. 1).

- The emulator constructed from nine FLAMINGO models is able to reproduce the results of the simulations with a relative error of less than 1% for scales up to $k = 10 h \cdot \text{Mpc}^{-1}$ and for all redshifts up to $z = 2$ (Figs. 2 & 3).

- The emulator requires less than 1 ms per invocation on a single compute core to provide the response at all k values. It can thus be used as part of a model inference exercise for surveys without penalty.

- The ‘fgas±Nσ’ input parameter to our model can be related to the gas fraction in groups/clusters and this latter quantity can be extracted from observations to serve as prior on the range of inputs to our emulator. The mapping between the two quantities for different halo masses is given in Fig. 4.

- We find the baryonic response to be stronger for models with lower gas fractions in groups and clusters (parameter ‘fgas±Nσ’, Fig. 5 & 6) and for lower stellar fractions (Fig. 8).

- The response is stronger, at fixed gas fractions in clusters, for the models using collimated AGN over thermal AGN feedback (Fig. 7).

- The baryonic response is stronger at lower redshift with the range of k -scales affected growing as the redshift decreases. Simultaneously, the position of the minimum of the response moves to larger k (Fig. 2).

- Models with stronger feedback (and thus a stronger response) display a larger evolution in their response between $z = 1$ and $z = 0$ (Fig. 9).

- The dependence of the response on the cosmological model is small ($< 1\%$ for all relevant k , Fig. 10) but we only probed two specific cosmological models, leaving room for a stronger dependence when other parameters are changed.

- By varying its input parameters, our emulator can cover a wide range of responses found in simulations from the literature (Fig. 11) except the most extreme models. The connection between our input parameters and the gas fraction in haloes also allows for a more physically meaningful description of the response, compared with the use of subgrid parameter values.

- Comparing our model to the model obtained from the ANTILLES simulations, we find that, even when using the simulated baryon fractions as input parameters, the SP(k) model does not match our results (Fig. 12). This indicates that more than one parameter is necessary to describe the baryonic response.

- When comparing our emulator to the constraints on the baryonic response derived from either the analysis of weak-lensing with halo models, baryonification models, or when combined with additional datasets, we find that the most extreme FLAMINGO models can match some of these constraints (Fig. 13). These models are, however, in tension with the cluster X-ray data used to constrain our fiducial model.

We plan to extend our emulator in the future to provide more independent variations in the gas and stellar fractions in clusters as well as including changes in cosmological parameters. This latter improvement will allow us to break free from the assumption that the baryonic response is separable from cosmology.

The emulator in its present form should nevertheless be sufficient for the analysis of current cosmological surveys where the separability assumption is still commonly made.

ACKNOWLEDGEMENTS

We thank Josh Borrow for merging, packaging, and releasing changes to the SWIFTEMULATOR package facilitating the construction and use of our emulator.

This work used the DiRAC@Durham facility managed by the Institute for Computational Cosmology on behalf of the STFC DiRAC HPC Facility (www.dirac.ac.uk). The equipment was funded by BEIS capital funding via STFC capital grants ST/K00042X/1, ST/P002293/1, ST/R002371/1 and ST/S002502/1, Durham University and STFC operations grant ST/R000832/1. DiRAC is part of the National e-Infrastructure.

DATA AVAILABILITY

The model introduced in this paper will be made fully publicly available on the FLAMINGO project’s web-page⁵ upon publication of this manuscript. The raw power-spectrum data used to construct the emulator will be made available upon reasonable request. The full FLAMINGO simulation data will eventually be made publicly available, though we note that the data volume (several petabytes) may prohibit us from simply placing the raw data on a server. In the meantime, people interested in using the simulations are encouraged to contact the corresponding author.

REFERENCES

- Abbott T. M. C., et al., 2022, *Phys. Rev. D*, **105**, 023520
 Abdalla E., et al., 2022, *Journal of High Energy Astrophysics*, **34**, 49
 Ambikasaran S., Foreman-Mackey D., Greengard L., Hogg D. W., O’Neil M., 2015, *IEEE Transactions on Pattern Analysis and Machine Intelligence*, **38**, 252
 Amon A., Efstathiou G., 2022, *MNRAS*, **516**, 5355
 Amon A., et al., 2023, *MNRAS*, **518**, 477
 Angulo R. E., Pontzen A., 2016, *MNRAS*, **462**, L1
 Angulo R. E., Zennaro M., Contreras S., Aricò G., Pellejero-Ibañez M., Stücker J., 2021, *MNRAS*, **507**, 5869
 Aricò G., Angulo R. E., Contreras S., Ondaro-Mallea L., Pellejero-Ibañez M., Zennaro M., 2021, *MNRAS*, **506**, 4070
 Aricò G., Angulo R. E., Zennaro M., Contreras S., Chen A., Hernández-Monteagudo C., 2023, *A&A*, **678**, A109
 Asgari M., et al., 2021, *A&A*, **645**, A104
 Asgari M., Mead A. J., Heymans C., 2023, *The Open Journal of Astrophysics*, **6**, 39
 Bagla J. S., Ray S., 2003, *New Astron.*, **8**, 665
 Bahé Y. M., et al., 2022, *MNRAS*, **516**, 167
 Bigwood L., et al., 2024, *MNRAS*, **534**, 655
 Bocquet S., Heitmann K., Habib S., Lawrence E., Uram T., Frontiere N., Pope A., Finkel H., 2020, *ApJ*, **901**, 5
 Booth C. M., Schaye J., 2009, *MNRAS*, **398**, 53
 Borrow J., Schaller M., Bower R. G., Schaye J., 2022, *MNRAS*, **511**, 2367
 Braspenning J., et al., 2024, *MNRAS*, **533**, 2656
 Chaikin E., Schaye J., Schaller M., Bahé Y. M., Nobels F. S. J., Ploeckinger S., 2022, *MNRAS*, **514**, 249
 Cheng H., Greengard L., Rokhlin V., 1999, *Journal of Computational Physics*, **155**, 468

⁵ <https://flamingo.strw.leidenuniv.nl/>

- Chisari N. E., et al., 2018, *MNRAS*, **480**, 3962
- Chisari N. E., et al., 2019, *The Open Journal of Astrophysics*, **2**, 4
- Correa C. A., Wyithe J. S. B., Schaye J., Duffy A. R., 2015, *MNRAS*, **452**, 1217
- van Daalen M. P., Schaye J., 2015, *MNRAS*, **452**, 2247
- van Daalen M. P., Schaye J., Booth C. M., Dalla Vecchia C., 2011, *MNRAS*, **415**, 3649
- van Daalen M. P., McCarthy I. G., Schaye J., 2020, *MNRAS*, **491**, 2424
- Dalla Vecchia C., Schaye J., 2008, *MNRAS*, **387**, 1431
- Davé R., Anglés-Alcázar D., Narayanan D., Li Q., Rafieferantsoa M. H., Appleby S., 2019, *MNRAS*, **486**, 2827
- DeRose J., et al., 2019, *ApJ*, **875**, 69
- Debackere S. N. B., Schaye J., Hoekstra H., 2020, *MNRAS*, **492**, 2285
- Delgado A. M., et al., 2023, *MNRAS*, **526**, 5306
- Dodelson S., Schmidt F., 2020, *Modern Cosmology*. Academic press, doi:10.1016/C2017-0-01943-2
- Driver S. P., et al., 2022, *MNRAS*, **513**, 439
- Elbers W., Frenk C. S., Jenkins A., Li B., Pascoli S., 2021, *MNRAS*, **507**, 2614
- Elbers W., Frenk C. S., Jenkins A., Li B., Pascoli S., 2022, *MNRAS*, **516**, 3821
- Elbers W., et al., 2024, *arXiv e-prints*, p. arXiv:2403.12967
- Euclid Collaboration et al., 2019, *MNRAS*, **484**, 5509
- Giri S. K., Schneider A., 2021, *J. Cosmology Astropart. Phys.*, **2021**, 046
- Hadzhiyska B., et al., 2024, *arXiv e-prints*, p. arXiv:2407.07152
- Hahn O., Rampf C., Uhlemann C., 2021, *MNRAS*, **503**, 426
- Heitmann K., et al., 2016, *ApJ*, **820**, 108
- Henden N. A., Puchwein E., Shen S., Sijacki D., 2018, *MNRAS*, **479**, 5385
- Heymans C., et al., 2021, *A&A*, **646**, A140
- Huško F., Lacey C. G., Schaye J., Schaller M., Nobels F. S. J., 2022, *MNRAS*, **516**, 3750
- Jenkins A., et al., 1998, *ApJ*, **499**, 20
- Jing Y. P., 2005, *ApJ*, **620**, 559
- Kay S. T., Braspenning J., Chluba J., Helly J. C., Kugel R., Schaller M., Schaye J., 2024, *MNRAS*, **534**, 251
- Kugel R., Borrow J., 2022, *The Journal of Open Source Software*, **7**, 4240
- Kugel R., et al., 2023, *MNRAS*, **526**, 6103
- Lahav O., Liddle A. R., 2022, *arXiv e-prints*, p. arXiv:2201.08666
- Lawrence E., et al., 2017, *ApJ*, **847**, 50
- Le Brun A. M. C., McCarthy I. G., Schaye J., Ponman T. J., 2014, *MNRAS*, **441**, 1270
- Lesgourgues J., 2011, *arXiv e-prints*, p. arXiv:1104.2932
- Lewis A., Challinor A., Lasenby A., 2000, *ApJ*, **538**, 473
- van Loon M. L., van Daalen M. P., 2024, *MNRAS*, **528**, 4623
- McCarthy I. G., Le Brun A. M. C., Schaye J., Holder G. P., 2014, *MNRAS*, **440**, 3645
- McCarthy I. G., Schaye J., Bird S., Le Brun A. M. C., 2017, *MNRAS*, **465**, 2936
- McCarthy I. G., Bird S., Schaye J., Harnois-Deraps J., Font A. S., van Waerbeke L., 2018, *MNRAS*, **476**, 2999
- McCarthy I. G., et al., 2023, *MNRAS*, **526**, 5494
- McCarthy I. G., et al., 2024, in prep.
- Mead A. J., Heymans C., Lombriser L., Peacock J. A., Steele O. I., Winther H. A., 2016, *MNRAS*, **459**, 1468
- Mead A. J., Tröster T., Heymans C., Van Waerbeke L., McCarthy I. G., 2020, *A&A*, **641**, A130
- Mead A. J., Brieden S., Tröster T., Heymans C., 2021, *MNRAS*, **502**, 1401
- Miyatake H., et al., 2023, *Phys. Rev. D*, **108**, 123517
- Mummery B. O., McCarthy I. G., Bird S., Schaye J., 2017, *MNRAS*, **471**, 227
- Pakmor R., et al., 2023, *MNRAS*, **524**, 2539
- Ploekinger S., Schaye J., 2020, *MNRAS*, **497**, 4857
- Preston C., Amon A., Efstathiou G., 2023, *MNRAS*, **525**, 5554
- Rampf C., Uhlemann C., Hahn O., 2021, *MNRAS*, **503**, 406
- Rasmussen C. E., Williams C. K. I., 2006, *Gaussian Processes for Machine Learning*. MIT press Cambridge, MA
- Salcido J., McCarthy I. G., Kwan J., Upadhye A., Font A. S., 2023, *MNRAS*, **523**, 2247
- Schaller M., et al., 2024, *MNRAS*, **530**, 2378
- Schaye J., Dalla Vecchia C., 2008, *MNRAS*, **383**, 1210
- Schaye J., et al., 2015, *MNRAS*, **446**, 521
- Schaye J., et al., 2023, *MNRAS*, **526**, 4978
- Schneider A., Teyssier R., 2015, *J. Cosmology Astropart. Phys.*, **2015**, 049
- Schneider A., Teyssier R., Stadel J., Chisari N. E., Le Brun A. M. C., Amara A., Refregier A., 2019, *J. Cosmology Astropart. Phys.*, **2019**, 020
- Schneider A., Giri S. K., Amodeo S., Refregier A., 2022, *MNRAS*, **514**, 3802
- Seljak U., 2000, *MNRAS*, **318**, 203
- Semboloni E., Hoekstra H., Schaye J., van Daalen M. P., McCarthy I. G., 2011, *MNRAS*, **417**, 2020
- Semboloni E., Hoekstra H., Schaye J., 2013, *MNRAS*, **434**, 148
- Smith R. E., et al., 2003, *MNRAS*, **341**, 1311
- Springel V., Di Matteo T., Hernquist L., 2005, *ApJ*, **620**, L79
- Springel V., et al., 2018, *MNRAS*, **475**, 676
- Storey-Fisher K., Tinker J. L., Zhai Z., DeRose J., Wechsler R. H., Banerjee A., 2024, *ApJ*, **961**, 208
- Takahashi R., Sato M., Nishimichi T., Taruya A., Oguri M., 2012, *ApJ*, **761**, 152
- Tröster T., et al., 2022, *A&A*, **660**, A27
- Villaescusa-Navarro F., et al., 2021, *ApJ*, **915**, 71
- Vogelsberger M., et al., 2014, *MNRAS*, **444**, 1518
- Wiersma R. P. C., Schaye J., Theuns T., Dalla Vecchia C., Tornatore L., 2009, *MNRAS*, **399**, 574

This paper has been typeset from a \LaTeX file prepared by the author.